

---

# BARYCENTRIC-ALIGNMENT AND RECONSTRUCTION LOSS MINIMIZATION FOR DOMAIN GENERALIZATION

---

**Boyang Lyu**

Department of Electrical and Computer Engineering  
Tufts University  
Medford, MA 02155  
Boyang.Lyu@tufts.edu

**Thuan Nguyen**

Department of Computer Science  
Tufts University  
Medford, MA 02155  
Thuan.Nguyen@tufts.edu

**Prakash Ishwar**

Department of Electrical and Computer Engineering  
Boston University  
Boston, MA 02215  
pi@bu.edu

**Matthias Scheutz**

Department of Computer Science  
Tufts University  
Medford, MA 02155  
Matthias.Scheutz@tufts.edu

**Shuchin Aeron**

Department of Electrical and Computer Engineering  
Tufts University  
Medford, MA 02155  
Shuchin@ece.tufts.edu

## ABSTRACT

Domain generalization theory and methods are important for the success of Open World Pattern Recognition. The paper advances the current state-of-art works in this context by proposing a novel theoretical analysis and piratical algorithm. In particular, we revisit Domain Generalization (DG) problem, where the hypotheses are composed of a common representation mapping followed by a labeling function. Popular DG methods optimize a well-known upper bound of the risk in the unseen domain to learn both the optimal representation and labeling functions. However, the widely used bound contains a term that is not optimized due to its dual dependence on the representation mapping and the unknown optimal labeling function in the unseen domain. To fill this gap, we derive a new upper bound free of terms having such dual dependence. Our derivation leverages old and recent *transport inequalities* that link optimal transport metrics with information-theoretic measures. Compared to previous bounds, our bound introduces two new terms: (i) the Wasserstein-2 barycenter term for the distribution alignment between domains and (ii) the reconstruction loss term for measuring how well the data can be reconstructed from its representation. Based on the new upper bound, we propose a novel DG algorithm that simultaneously minimizes the classification loss, the barycenter loss, and the reconstruction loss. Experiments on several datasets demonstrate superior performance of the proposed method compared to the state-of-the-art DG algorithms.

## 1 INTRODUCTION

In many real-world applications of modern machine learning, the training (seen) data and the test (unseen) data may belong to different *domains*, leading to the loss of predictive power of the learned models. For example, a model trained on data from one hospital may not work well when the test data is from another hospital [18], a drowsiness driving estimator trained on one group of subjects does not generalize well for other subjects [9], a cognitive workload estimator from fNIRS (functional near-infrared spectroscopy) measurements may not generalize well across sessions and subjects [27].

These types of problems are broadly classified into two categories, viz., Domain Adaptation (DA) [5] and Domain Generalization (DG) [7]. Both DA and DG aim to find a model that can generalize well when the training data from the seen domain does not share the same distribution as the testing data from the unseen domain. The key difference between DA and DG is that DA allows access to the (unlabeled) unseen domain data during the training process while DG does not, leading to a more challenging problem. Both DG and DA have a close relationship with Transfer Learning [42], all of which aim to enhance the robustness of the learned model. For an extensive survey and related literature, we refer the reader to the excellent recent survey [42].

To address the problem of DG, motivated by the seminal theoretical works of [5, 4], one usually parameterizes the hypothesis as composed of a representation function followed by a labeling function [2, 12, 25, 41]. The essential insight from the upper bound derived in [5, 4] is that the risk on the unseen domain is upper bounded by three terms: (1) the prediction risk on the mixture of seen domains, (2) discrepancy or divergence between the data distributions in the representation space, and (3) a *combined risk* across all domains that is implicitly dependent on both the representation map and the unknown optimal labeling function from the unseen domain. Due to this dual dependency, most existing works ignore optimizing the third term (*combined risk*) and treat it as a constant for a given representation map. Ignoring the *combined risk*, a large body of the DG (as well as DA) methods [25, 17, 39] are essentially based on a variation of the following theme - learn a domain invariant representation mapping *or* align the domains in the representation space, together with learning a common labeling function controlling the prediction loss across the seen domains. However, it is worth noticing that the *combined risk* is actually a function of the representation map and hence needs to be part of the optimization. A detailed analysis of the shortcomings of the previous studies is provided in our Appendix A.1.

## 1.1 Main Contributions

In this paper, by revisiting the seminal works in [5, 4], we derive a new upper bound for the risk of unseen domain with four terms: (1) the prediction risk across seen domains in the input space; (2) the discrepancy/divergence between the induced distributions of seen and unseen domains in representation space, which can be expressed in terms of the Wasserstein-2 Barycenter [32] of the seen domains; (3) the reconstruction loss term that measures how well the input can be reconstructed from its representation; and (4) a *combined risk* term that is a constant with respect to the representation map and the labeling function to be learned. A detailed comparison between previous bounds and our work can be found in Appendix A.1.

Finally, based on these theoretical insights, we propose a new algorithm named Wasserstein Barycenter Auto-Encoder (WBAE). The proposed algorithm leverages recent advances in the fast and efficient computation of Wasserstein barycenters and utilizes the encoder-decoder structure for minimizing the reconstruction loss.

## 1.2 Related Work

Our work is closely related to the work that aims to learn the domain invariant features by decomposing the prediction function into a representation function followed by a classifier. For example, in [2], the authors propose a model consisting of three parts: a feature extractor, a classifier, and domain discriminators. The feature extractor learns the task-sensitive but domain-invariant features via minimizing the cross-entropy loss w.r.t the task label and maximizing the sum of domain discriminator loss. The domain discriminator loss is treated as an estimation of  $\mathcal{H}$  divergence between all seen domains [4], which has its roots in the works [17, 26] from the Domain Adaptation area. Following a similar idea, [25] align the representation distributions from different domains via minimizing their maximum mean discrepancy. In [12], the authors adopt a gradient-based episodic training scheme for DG, the extracted features are enforced to retain the global class relationship and the local task-related clusters via minimizing alignment loss between soft-confusion matrices and contrastive loss. [3] propose Invariant Risk Minimization algorithm to learn features such that the optimal classifiers on top are matched across domains. [28] consider different styles of different domains as the main factor causing the domain gap, and achieve DG by disentangling it from learned features. Among the large body of works on the DG problem, we consider [6, 17, 22, 26, 3] as recent exemplars of principled algorithms guided by theory and we mainly focus on comparing the performance of our methods against methods from these papers.

Since our proposed upper bound is based on the Wasserstein distance, it is worth mentioning the work proposed in [31, 33, 41]. Specifically, [41] use the pairwise Wasserstein-1 distance [29, 32] to estimate the divergence between different seen domains. Using the dual form of the Wasserstein-1 distance, the feature extractor in [41] minimizes a combination of cross-entropy loss, Wasserstein distance loss, and a contrastive loss to achieve DG. On the other hand, [31, 33] are designed for DA problem and constructed based on the Wasserstein-1 distance. Even though the bounds from [31, 33] share some similarities with ours, their bounds are constructed on the input space and therefore do not explicitly motivate the use of representation functions.

## 2 THEORETICAL ANALYSIS AND PROPOSED METHODS

We consider a *domain*  $v$  as a triple  $(\mu^{(v)}, f^{(v)}, g^{(v)})$  consisting of a distribution  $\mu^{(v)}$  on the inputs  $\mathbf{x} \in \mathbb{R}^d$ , a representation function  $f^{(v)} : \mathbb{R}^d \rightarrow \mathbb{R}^{d'}$ ,  $d' \leq d$ , from the input space to the representation space, and a stochastic labeling function  $g^{(v)} : \mathbb{R}^{d'} \rightarrow \mathcal{Y}$  from the representation space to the label space. We denote the unseen domain by  $(\mu^{(u)}, f^{(u)}, g^{(u)})$  and  $S$  seen domains by  $(\mu^{(s)}, f^{(s)}, g^{(s)})$ ,  $s = 1, \dots, S$ .

Let  $\mathcal{F} = \{f|f : \mathbb{R}^d \rightarrow \mathbb{R}^{d'}\}$  be the set of *representation functions*,  $\mathcal{G} = \{g|g : \mathbb{R}^{d'} \rightarrow \mathcal{Y}\}$  be the set of stochastic *labeling functions*,  $\mathcal{H} := \mathcal{G} \circ \mathcal{F}$  be the set of *hypotheses*, with each hypothesis  $h : \mathbb{R}^d \rightarrow \mathcal{Y}$  obtained by composing each  $g \in \mathcal{G}$  with each  $f \in \mathcal{F}$ , i.e.,  $h = g \circ f$ , and  $\mathcal{D} = \{\psi|\psi : \mathbb{R}^{d'} \rightarrow \mathbb{R}^d\}$  be the set of *reconstruction functions* that map from the representation space back to the input space. In this paper, we limit our theoretical study to binary classification problems i.e., we only consider the hypothesis functions  $h$  such that  $h : \mathbb{R}^d \rightarrow \mathcal{Y} = [0, 1]$ . Note that a similar setup is also used in [5] where the hypothesis  $h$  occurs non-deterministically and maps a data point to a label between zero and one.

The risk of using a hypothesis  $h$  in domain  $v$  is defined by:

$$R^{(v)}(h) := \mathbb{E}_{\mathbf{x} \sim \mu^{(v)}} [\ell(h(\mathbf{x}), h^{(v)}(\mathbf{x}))] \quad (1)$$

where  $\mathbb{E}[\cdot]$  denotes expectation,  $h^{(v)} = g^{(v)} \circ f^{(v)}$ , and  $\ell(\cdot, \cdot)$  is a loss function. Next, we make the following assumptions:

**A1:** The loss function  $\ell(\cdot, \cdot)$  is non-negative, symmetric, bounded by a finite positive number  $L$ , satisfies the triangle inequality, and  $Q$ -Lipschitz continuous. Specifically, we assume that for any  $a, b, c$  and a positive constant  $Q$ , the following inequality holds:

$$|\ell(a, b) - \ell(a, c)| \leq Q \|b - c\|_2, \quad (2)$$

where  $\|b - c\|_2$  denotes the Euclidean distance between  $b$  and  $c$ .

**A2:** The optimal hypothesis on unseen domain  $h^{(u)} = g^{(u)} \circ f^{(u)}$  is  $K$ -Lipschitz continuous. Specifically, we assume that for any  $a, b$ , and a positive constant  $K$ , the following inequality holds:

$$|h^{(u)}(a) - h^{(u)}(b)| \leq K \|a - b\|_2. \quad (3)$$

The first four conditions in Assumption A1 can be easily satisfied by any metric or norm truncated by a finite positive number. Concretely, if  $d(a, b)$  is a metric, potentially unbounded like Mean Squared Error (MSE), then  $loss(a, b) := \min(L, d(a, b))$  satisfies the first four conditions in A1. In addition, the Lipschitzness assumption in both Assumption A1 and A2 is widely used in many DG works [6, 33, 37] and in practice, Assumption A2 can be approximately satisfied by neural networks with a gradient penalty [33].

One may find our assumptions bear some similarities with the assumptions in [31] and [33], but there are some fundamental differences. Specifically, we assume that the loss function is non-negative, symmetric, bounded, Lipschitz, and satisfies the triangle inequality, while the loss function in [31] is required to be convex, symmetric, bounded, obeying the triangle inequality, and satisfying a specific form. On the other hand, we only assume that the optimal hypothesis function on the unseen domain is Lipschitz, while [33] requires all hypotheses to be Lipschitz.

### 2.1 Bound for Unseen Domain Risk

We begin by considering a single seen domain. Lemma 2.1 below upper bounds the risk  $R^{(u)}(h)$  of a hypothesis  $h = g \circ f$  in the unseen domain  $u$  by four terms: (1) the first term is the risk in a *single* seen domain  $s$ , (2) the second term is the  $L^1$  distance between the distributions of the *data representations* from the seen and unseen domain, (3) the third term measures how well the input can be reconstructed from its corresponding representation, and (4) the fourth term is an intrinsic risk term that is free of  $h$  and is intrinsic to the domains and the loss function. We use the notation  $f_{\#}\mu^{(v)}$  to denote the pushforward of distribution of  $\mu^{(v)}$ , i.e., the distribution of  $f(\mathbf{x})$  with  $\mathbf{x} \sim \mu^{(v)}$ .

**Lemma 2.1.** *Under assumptions A1 and A2, for any hypothesis  $h \in \mathcal{H}$  and any reconstruction function  $\psi \in \mathcal{D}$ , the following bound holds:*

$$R^{(u)}(h) \leq R^{(s)}(h) + L \|f_{\#}\mu^{(u)} - f_{\#}\mu^{(s)}\|_1 + QK \left( \mathbb{E}_{\mathbf{x} \sim \mu^{(s)}} [\|\psi(f(\mathbf{x})) - \mathbf{x}\|_2] + \mathbb{E}_{\mathbf{x} \sim \mu^{(u)}} [\|\psi(f(\mathbf{x})) - \mathbf{x}\|_2] \right) + \sigma^{(u,s)}$$

where  $\|f_{\#}\mu^{(u)} - f_{\#}\mu^{(s)}\|_1 = \int_{\mathbf{z}} |f_{\#}\mu^{(u)} - f_{\#}\mu^{(s)}| dz$  denotes the  $L^1$  distance between  $(f_{\#}\mu^{(u)}, f_{\#}\mu^{(s)})$  in the representation space and:

$$\sigma^{(u,s)} := \min \{ \mathbb{E}_{\mathbf{x} \sim \mu^{(u)}} [\ell(h^{(u)}(\mathbf{x}), h^{(s)}(\mathbf{x}))], \mathbb{E}_{\mathbf{x} \sim \mu^{(s)}} [\ell(h^{(u)}(\mathbf{x}), h^{(s)}(\mathbf{x}))] \}.$$

*Proof.* Please see Appendix B.1.  $\square$

In typical applications of DG, training data from multiple seen domains are available, which can be mixed in myriad ways. Lemma 2.2 below, therefore, extends Lemma 2.1 to a convex combination of distributions of seen domains.

**Lemma 2.2.** *For any convex weights  $\lambda^{(1)}, \lambda^{(2)}, \dots, \lambda^{(S)}$  (nonnegative and summing to one), any reconstruction function  $\psi \in \mathcal{D}$ , and any hypothesis  $h \in \mathcal{H}$ , the following bound holds:*

$$\begin{aligned} R^{(u)}(h) &\leq \sum_{s=1}^S \lambda^{(s)} R^{(s)}(h) + L \sum_{s=1}^S \lambda^{(s)} \|f_{\#}\mu^{(u)} - f_{\#}\mu^{(s)}\|_1 \\ &+ QK \left( \sum_{s=1}^S \lambda^{(s)} \mathbb{E}_{\mathbf{x} \sim \mu^{(s)}} [\|\psi(f(\mathbf{x})) - \mathbf{x}\|_2] + \mathbb{E}_{\mathbf{x} \sim \mu^{(u)}} [\|\psi(f(\mathbf{x})) - \mathbf{x}\|_2] \right) + \sum_{s=1}^S \lambda^{(s)} \sigma^{(u,s)}. \end{aligned}$$

*Proof.* This follows immediately by taking the convex combination of the bound given by Lemma 2.1 over the seen domains.  $\square$

The upper bound is based on the  $L^1$  distances between the pushforwards of seen and unseen distributions. Estimating  $L^1$  distances accurately from samples is well-known to be hard [4, 19]. To overcome this practical limitation, we upper bound the  $L^1$  distance by the Wasserstein-2 distance under additional regularity assumptions on the pushforwards.

**Definition 2.3.** [30] A probability distribution on  $\mathbb{R}^d$  is called  $(c_1, c_2)$ -regular, with  $c_1, c_2 \geq 0$ , if it is absolutely continuous with respect to the Lebesgue measure with a differentiable density  $p(\mathbf{x})$  such that

$$\forall \mathbf{x} \in \mathbb{R}^d, \quad \|\nabla \log_2 p(\mathbf{x})\|_2 \leq c_1 \|\mathbf{x}\|_2 + c_2,$$

where  $\nabla$  denotes the gradient and  $\|\cdot\|_2$  denotes the standard Euclidean norm.

**Lemma 2.4.** *If  $\mu$  and  $\nu$  are  $(c_1, c_2)$ -regular, then*

$$\|\mu - \nu\|_1 \leq \sqrt{c_1 \left( \sqrt{\mathbb{E}_{\mathbf{u} \sim \mu} [\|\mathbf{u}\|_2^2]} + \sqrt{\mathbb{E}_{\mathbf{v} \sim \nu} [\|\mathbf{v}\|_2^2]} \right) + 2c_2} \times \sqrt{W_2(\mu, \nu)}$$

where the Wasserstein- $p$  metric [29, 32]  $W_p(\mu, \nu)$  is defined as,

$$W_p(\mu, \nu) := \left( \inf_{\pi \in \Pi(\mu, \nu)} \mathbb{E}_{(\mathbf{u}, \mathbf{v}) \sim \pi} [\|\mathbf{u} - \mathbf{v}\|_2^p] \right)^{1/p}$$

where  $\Pi(\mu, \nu)$  is the set of joint distributions with marginals  $\mu$  and  $\nu$ .

*Proof.* Please see Appendix B.2.  $\square$

One may ask: what conditions guarantee the regularity of the pushforward distributions? Proposition 2 and Proposition 3 in [30] show that any distribution  $\nu$  for which  $\mathbb{E}_{\mathbf{v} \sim \nu} \|\mathbf{v}\|_2$  is finite becomes regular when convolved with any regular distribution, including the Gaussian distribution. Since convolution of distributions corresponds to addition of independent random vectors having those distributions, in practice it is always possible to make the pushforwards regular by adding a small amount of independent spherical Gaussian noise in representation space.

Combining Lemma 2.2, Lemma 2.4, and Jensen's inequality, we obtain our main result:

**Theorem 2.5.** *If  $f_{\#}\mu^{(s)}$ ,  $s = 1, 2, \dots, S$ , and  $f_{\#}\mu^{(u)}$  are all  $(c_1, c_2)$ -regular, then for any convex weights  $\lambda^{(1)}, \lambda^{(2)}, \dots, \lambda^{(S)}$ , any reconstruction function  $\psi \in \mathcal{D}$ , and any hypothesis  $h \in \mathcal{H}$ , the following bound holds:*

$$\begin{aligned} R^{(u)}(h) &\leq \sum_{s=1}^S \lambda^{(s)} R^{(s)}(h) + LC \left[ \sum_{s=1}^S \lambda^{(s)} W_2^2(f_{\#}\mu^{(u)}, f_{\#}\mu^{(s)}) \right]^{1/4} \\ &+ QK \left( \sum_{s=1}^S \lambda^{(s)} \mathbb{E}_{\mathbf{x} \sim \mu^{(s)}} [\|\psi(f(\mathbf{x})) - \mathbf{x}\|_2] + \mathbb{E}_{\mathbf{x} \sim \mu^{(u)}} [\|\psi(f(\mathbf{x})) - \mathbf{x}\|_2] \right) + \sum_{s=1}^S \lambda^{(s)} \sigma^{(u,s)} \quad (4) \end{aligned}$$

where:

$$C = \max_s \sqrt{c_1 \left( \sqrt{\mathbb{E}_{\mathbf{x} \sim \mu^{(u)}} [\|f(\mathbf{x})\|_2^2]} + \sqrt{\mathbb{E}_{\mathbf{x} \sim \mu^{(s)}} [\|f(\mathbf{x})\|_2^2]} \right) + 2c_2}.$$

*Proof.* Please see Appendix B.3. □

The upper bound in Theorem 2.5 is composed by four terms: the first term is the sum of the risk on seen domains, the second term is the Wasserstein distance between the push-forward of seen and unseen domains in the representation space, the third term indicates how well the input can be reconstructed from its corresponding representation, and the fourth term is independent of both the representation function and the labeling function and only intrinsic to the domain and loss function.

One may find the form of the upper bound derived above shares some similarities with previous bounds in [5, 31, 33]. However, our bound can be distinguished based on the following key points:

- First, though Lemma 1 in [31] and Theorem 1 in [33] also introduce Wasserstein distance between domain distributions as our second term in Theorem 2.5. However:
  1. Our second term (for capturing domain divergence) is constructed in the *representation* space, not in the data (ambient) space, which provides a theoretical justification for the risk of unseen domain when decomposing the hypothesis into a representation mapping and a labeling function. This is also consistent with the algorithm implementation in practice.
  2. The bounds in Lemma 1 of [31] and Theorem 1 of [33] are controlled by the Wasserstein-1 distance, while our upper bound is managed by the square root of the Wasserstein-2 distance. There are regimes where one bound is tighter than the other. Please see the detailed analysis in Appendix A.2.
- Second, our third term measures how well the input can be reconstructed from its representation. This motivates the use of an encoder-decoder structure in the proposed algorithm in Sec. 3 to minimize the reconstruction loss, which is novel compared with the previous works [5, 31, 33].
- Finally, the last term in our upper bound is independent of both the representation function  $f$  and the labeling function  $g$ . This contrasts with the previous results in [5], where the last term in their upper bound (see Theorem 1 in [5]) depends on the representation function  $f$ . Please refer to Appendix A.1 for the detailed comparison.

The bound proposed in Theorem 2.5 can also be used for the DA problem where one can access the unseen/target domain data and estimate its distribution. However, under the DG setting, the second and third term in Eq. (4) are uncontrollable, leading to an intractable upper bound due to the unavailability of the unseen data. Without making additional specific assumptions on the unseen domain, this intractability can not be overcome, which is also widely treated as a fundamental problem of DG.

As a step toward developing a practical algorithm based on our new bound, we decompose both the second term and the third term in Eq. (4) into two separate terms where one completely depends on the unseen distribution and the other fully depends on the seen distributions.

**Corollary 2.6.** *Using the notations in Theorem 2.5, for an arbitrary pushforward distribution  $f_{\#}\mu$ , we have:*

$$\begin{aligned}
 R^{(u)}(h) &\leq \sum_{s=1}^S \lambda^{(s)} R^{(s)}(h) + LC \left( \sum_{s=1}^S \lambda^{(s)} W_2^2(f_{\#}\mu, f_{\#}\mu^{(s)}) \right)^{1/4} + LC \left( W_2^2(f_{\#}\mu^{(u)}, f_{\#}\mu) \right)^{1/4} \\
 &+ QK \left( \sum_{s=1}^S \lambda^{(s)} \mathbb{E}_{\mathbf{x} \sim \mu^{(s)}} [\|\psi(f(\mathbf{x})) - \mathbf{x}\|_2] \right) + QK \left( \mathbb{E}_{\mathbf{x} \sim \mu^{(u)}} [\|\psi(f(\mathbf{x})) - \mathbf{x}\|_2] \right) + \sum_{s=1}^S \lambda^{(s)} \sigma^{(u,s)}. \quad (5)
 \end{aligned}$$

*Proof.* Please see Appendix B.4. □

Motivated by the bound in Corollary 2.6, we want to find a suitable representation function  $f$  together with a reconstruction function  $\psi$  to minimize the second term  $\sum_{s=1}^S \lambda^{(s)} W_2^2(f_{\#}\mu, f_{\#}\mu^{(s)})$  and the fourth term  $\sum_{s=1}^S \lambda^{(s)} \mathbb{E}_{\mathbf{x} \sim \mu^{(s)}} [\|\psi(f(\mathbf{x})) - \mathbf{x}\|_2]$  in Eq. (5), while ignoring the third term  $W_2^2(f_{\#}\mu^{(u)}, f_{\#}\mu)$  and the fifth term  $\mathbb{E}_{\mathbf{x} \sim \mu^{(u)}} [\|\psi(f(\mathbf{x})) - \mathbf{x}\|_2]$  since both of them are completely intractable.

Minimizing the second term  $\sum_{s=1}^S \lambda^{(s)} W_2^2(f_{\#}\mu, f_{\#}\mu^{(s)})$  in Eq. (5) leads to finding the Wasserstein-2 barycenter of the distributions of seen domains in the representation space. Here, we assume a uniform weights for all domains, *i.e.*, assuming  $\lambda^{(s)} = \frac{1}{S}, \forall s$ , since there is no additional information for selecting the weights of the seen domains.

Particularly, the Wasserstein-2 barycenter of the pushforward distributions of seen domains is defined by:

$$f_{\#}\mu_{barycenter} := \arg \min_{f_{\#}\mu} \sum_{s=1}^S \frac{1}{S} W_2^2(f_{\#}\mu^{(s)}, f_{\#}\mu). \quad (6)$$

We refer the reader to [1, 11] for the definition and properties (existence, uniqueness) of the Wasserstein barycenter.

On the other hand, minimizing the fourth term  $\sum_{s=1}^S \lambda^{(s)} \mathbb{E}_{\mathbf{x} \sim \mu^{(s)}} [\|\psi(f(\mathbf{x})) - \mathbf{x}\|_2]$  in Eq. (5) naturally leads to an Auto-Encoder mechanism. With a little abuse of notation, we denote the encoder, namely the representation function as  $f$  and the decoder, namely the reconstruction function as  $\psi$ . The  $L^2$  reconstruction loss should be optimized over all seen domains.

## 2.2 Proposed Method

Since the last term in Corollary 2.6 is independent of both the representation function  $f$  and the labeling function  $g$ , while the third and the fifth terms in Corollary 2.6 are intractable due to their dependence on unseen domain, we thus focus on designing  $f$ ,  $\psi$  and  $g$  to minimize the first, the second, and the fourth terms in Eq. (5), Corollary 2.6.

Following previous work [2, 4, 5], we optimize the first term by training  $f$  together with  $g$  using a standard cross-entropy (CE) loss, such that the empirical classification risk on seen domains is minimized. The classification loss function can be written as:

$$L_c(f, g) = \sum_{s=1}^S \mathbb{E}_{\mathbf{x} \sim \mu^{(s)}} [\text{CE}(h^{(s)}(\mathbf{x}), g(f(\mathbf{x})))] \quad (7)$$

where  $\text{CE}(h^{(s)}(\mathbf{x}), g(f(\mathbf{x})))$  denotes the cross entropy (CE) loss between the output of classifier and the ground-truth label of seen domain  $s$ .

As discussed in Corollary 2.6, we propose to use the Wasserstein-2 barycenter of representation distributions of seen domains to optimize the second term in Eq. (5). Specifically, the barycenter loss is defined by:

$$L_{bary}(f) := \sum_{s=1}^S \frac{1}{S} W_2^2(f_{\#}\mu^{(s)}, f_{\#}\mu_{barycenter}) \quad (8)$$

where  $f_{\#}\mu_{barycenter}$ , as defined in Eq. (6), denotes the Wasserstein barycenter of pushforward distributions of seen domains.

In contrast to the previous Wasserstein distance-based method [41] where pairwise Wasserstein distance loss is employed, we motivate the use of Wasserstein barycenter loss based on our Corollary 2.6 and demonstrate its ability in enforcing domain-invariance in the ablation study. Note that from the definition in (8), computing barycenter loss only requires computing  $S$  Wasserstein distances in contrast to  $S(S-1)/2$  when using pairwise Wasserstein distance.

Furthermore, to handle the fourth term in Eq. (5), an auto-encoder structure is utilized. Specifically, a decoder  $\psi: \mathbb{R}^{d'} \rightarrow \mathbb{R}^d$  is adopted, leading to the following reconstruction loss term:

$$L_r(f, \psi) := \sum_{s=1}^S \mathbb{E}_{\mathbf{x} \sim \mu^{(s)}} [\|\mathbf{x} - \psi(f(\mathbf{x}))\|_2^2]. \quad (9)$$

From the analysis above, we aim to find a representation function  $f$ , a classifier  $g$ , and a decoder function  $\psi$  to optimize the following objective function:

$$\arg \min_{f, g, \psi} L_c(f, g) + \alpha L_{bary}(f) + \beta L_r(f, \psi) \quad (10)$$

where weights  $\alpha, \beta > 0$  are hyperparameters. One can observe that the terms in our proposed upper bound are incorporated into our objective function in Eq. (10). Specifically, the first term in our objective function aims to determine a good classifier  $g$  together with a representation mapping  $f$  by minimizing the risk of seen domains, which corresponds to the first term of the upper bound in Eq. (5). The second term in our objective function acts as a domain alignment tool to minimize the discrepancy between seen domains, aligning with the second term in Eq. (5). Note that although  $L_{bary}$  itself requires solving an optimization problem, we leverage fast computation methods, which are also discussed in Section 3, to directly estimate this loss without invoking the Kantorovich-Rubenstein dual characterization of Wasserstein distances [32]. This avoids solving a min-max type problem that is often plagued by unstable numerical dynamics. Finally, the third term in the objective function minimizes the mean squared error between the input and its reconstruction over all seen domains, which directly minimizes the fourth term in Eq. (5).

### 3 ALGORITHMS

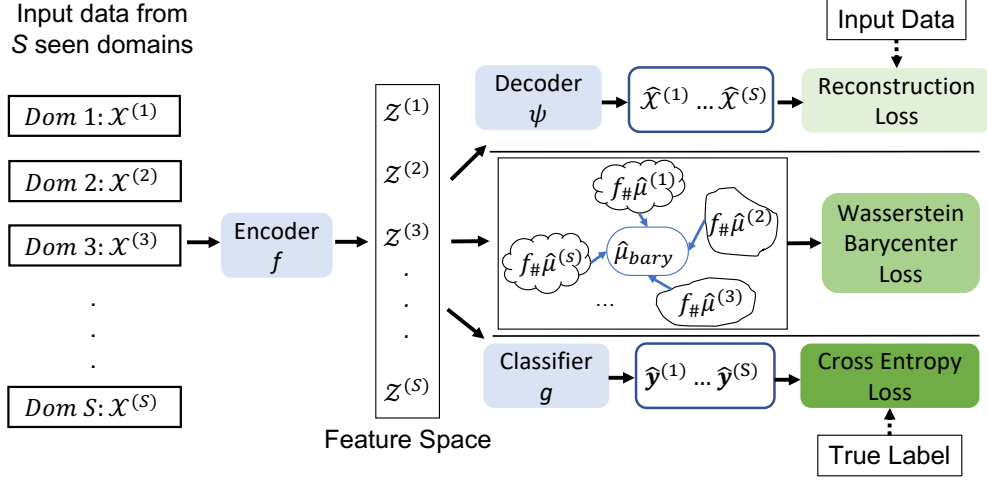


Figure 1: An overview of the proposed algorithm. The top, middle, and bottom branches refer to the reconstruction loss term, the Wasserstein barycenter loss term, and the classification risk (from seen domains), respectively.

Based on the loss function designed above, we propose an algorithm named Wasserstein Barycenter Auto-Encoder (WBAE). The pseudo code of the WBAE algorithm can be found in Algorithm 1 while its block diagram is shown in Figure 1.

---

#### Algorithm 1 Wasserstein Barycenter Auto-Encoder (WBAE)

---

**Input:** Data from  $S$  seen domains,  $m$  samples from each domain, learning rate  $\eta$ , parameters  $\alpha, \beta, \epsilon$ . **Output:** Encoder  $f_{\theta_e}$ , decoder  $\psi_{\theta_d}$ , classifier  $g_{\theta_c}$ .

- 1: **while** training is not end **do**
  - 2: Randomly choose  $m$  samples from each domain, denoted as  $\mathcal{X}^{(s)} := \{\mathbf{x}_i^{(s)}\}_{i=1}^m \sim \hat{\mu}^{(s)}$  and  $\mathbf{y}^{(s)} := \{y_i^{(s)}\}_{i=1}^m$
  - 3: **for**  $s = 1 : S$  and  $i = 1 : m$  **do**
  - 4:  $\mathbf{z}_i^{(s)} \leftarrow f_{\theta_e}(\mathbf{x}_i^{(s)})$  with set  $\mathcal{Z}^{(s)} \sim f_{\#}\hat{\mu}^{(s)}$
  - 5: **end for**
  - 6: Calculate the Wasserstein barycenter  $\hat{\mu}_{bary}$  of  $\{f_{\#}\hat{\mu}^{(s)}\}_{s=1}^S$  and its supporting points with  $f_{\theta_e}$  detached from automatic backpropagation:
  - 7:  $L_{bary} \leftarrow \frac{1}{S} \sum_{s=1}^S Sinkhorn_{\epsilon}(\hat{\mu}_{bary}, f_{\#}\hat{\mu}^{(s)})$
  - 8:  $L_c \leftarrow -\frac{1}{mS} \sum_{s=1}^S \sum_{i=1}^m y_i^s \log p(g_{\theta_c}(f_{\theta_e}(\mathbf{x}_i^{(s)})))$
  - 9:  $L_r \leftarrow \frac{1}{mS} \sum_{s=1}^S \sum_{i=1}^m \|\mathbf{x}_i^{(s)} - \psi_{\theta_d}(\mathbf{z}_i^{(s)})\|_2^2$
  - 10:  $L \leftarrow L_c + \alpha L_{bary} + \beta L_r$
  - 11:  $\theta_c \leftarrow \theta_c - \eta \nabla_{\theta_c} L_c$
  - 12:  $\theta_d \leftarrow \theta_d - \eta \nabla_{\theta_d} L_r$
  - 13:  $\theta_e \leftarrow \theta_e - \eta \nabla_{\theta_e} L$
  - 14: **end while**
- 

As shown in the pseudo code, we use an encoder  $f$  and a decoder  $\psi$ , which are parameterized by  $\theta_e$  and  $\theta_d$ , for feature extraction and reconstruction. Here  $\mathcal{X}^{(s)}$  is denoted as a set of samples from domain  $s$  with empirical distribution  $\hat{\mu}^{(s)}$  and with  $\mathbf{x}_i^{(s)}$  as one of its element. The corresponding label set of  $\mathcal{X}^{(s)}$  is  $\mathbf{y}^{(s)}$ , where  $\mathbf{y}^{(s)} := \{y_i^{(s)}\}$  with  $y_i^{(s)}$  is the label for sample  $\mathbf{x}_i^{(s)}$ . The extracted feature  $\mathbf{z}_i^{(s)} = f_{\theta_e}(\mathbf{x}_i^{(s)})$  in set  $\mathcal{Z}^{(s)}$  is under the empirical distribution of  $f_{\#}\hat{\mu}^{(s)}$ . The decoder takes the extracted features as input and outputs the reconstructions as  $\psi_{\theta_d}(\mathbf{z}_i^{(s)})$  for domain  $s$ . The classifier  $g$ , which is parameterized by  $\theta_c$  is applied to the extracted features for label prediction.

The proposed algorithm requires calculating Wasserstein-2 barycenter and its supporting points. Here we use an off-the-shelf python package [16] that implements a free-support Wasserstein barycenter algorithm described in [11]. This algorithm is executed in the primal domain and avoids the use of the dual form of Wasserstein distances, which

otherwise would turn the problem into an adversarial (min-max) type setting that we want to avoid due to its instability. The barycenter loss is approximated via an average Sinkhorn divergence [15] between the seen domains and the estimated barycenter. Sinkhorn divergence is an unbiased proxy for the Wasserstein distance, which leverages entropic regularization [10] for computational efficiency, thereby allowing for integrating automatic differentiation with GPU computation. We adopt the implementation in [15] to our algorithm for a fast gradient computation and denote it as  $Sinkhorn_\epsilon$  in Algorithm 1, where  $\epsilon$  is the entropic regularization term.

## 4 EXPERIMENTS AND RESULTS

The proposed method was evaluated on four widely used DG datasets: Colored MNIST [3], PACS [24], VLCS [14], and Office-Home [36] and compared with various *theory-guided* DG algorithms. We implemented the proposed method following Gulrajani’s work [18] and their DomainBed suite to facilitate the comparison with the results reported therein.

**Datasets:** The details for the four datasets are described below:

- **Colored MNIST dataset [3]:** Colored MNIST is derived from the MNIST handwritten digit dataset [23], where all 70,000 gray-scale images of the MNIST dataset are colored with either red or green in a way that the colors are spuriously correlated with the label of digits. The classification task is to identify whether the digits are less than five ( $< 5$ ) or greater (equal) than five ( $\geq 5$ ). Three domains are constructed by varying the correlation between the colors and the labels of images.
- **PACS dataset [24]:** PACS contains 9,991 images with 7 classes from 4 domains: Art (A), Cartoons (C), Photos (P) and Sketches (S), where each domain represents one type of images.
- **VLCS dataset [14]:** VLCS consists of 10,729 images from 4 different domains: VOC2007 (V), LabelMe (L), Caltech (C), PASCAL (S). A total of 5 classes are shared by all domains.
- **Office-Home dataset [36]:** Office-Home contains 15,500 images from 4 different domains: Artistic (A), Clipart (C), Product (P), and Real-World (R). Each domain has 65 object categories.

**Model Structure:** We used the same feature extractors and classifiers as described in DomainBed [18] for all four datasets. Specifically, an ImageNet pre-trained ResNet-50 model with the final (softmax) layer removed is used as the feature extractor for PACS, VLCS, and Office-Home datasets while MNIST ConvNet [18] is used for the Colored MNIST dataset. The decoder is a stack of 6 ConvTranspose2d layers for all non-MNIST datasets and 5 ConvTranspose2d layers for Colored MNIST dataset. The detailed structure of the decoders are described in Table 6 and 7 within Appendix C. The classifier is a one-linear-layer model with the output dimension the same as the number of classes.

**Hyper-parameters:** Due to the limitation of computational resources, we set all hyper-parameters (e.g., learning rate, batch size, dropout, etc.) to the default values shown in Table 6 of [18] and use the Adam optimizer [20] for optimization. The values of  $\epsilon$  for the Sinkhorn loss (line 7, Algorithm 1) is empirically set to 20 without tuning. We only tune two hyper-parameters, namely the weights  $\alpha$  and  $\beta$  (see Eq. (10)). As done in DomainBed [18], a random search of 20 trials is performed within the distribution of  $10^{\text{Uniform}[-3.5, -2]}$  for  $\alpha$  and  $10^{\text{Uniform}[-3.5, -1.5]}$  for  $\beta$ . A complete list of all hyper-parameters is shown in Table 8 in Appendix C.

**Model Selection:** We adopted the commonly used training-domain validation strategy in [18, 22] for hyper-parameter tuning and model selection. Specifically, we split the data from each domain into training and validation sets in the proportion 80% and 20%, respectively. During training, we aggregated together the training/validation samples from each seen domain to form the overall training/validation set and selected the model with the highest validation accuracy for testing.

**Model Evaluation:** We followed the commonly used leave-one-domain-out evaluation strategy [18, 12]: one domain is left out as the unseen test domain and the remaining domains are treated as the seen domains. Following [18], hyper-parameters were re-optimized for every new test unseen domain.

**Comparison Methods:** In this paper, we compare the empirical performance of our proposed method against the state-of-the-art DG methods reported in [18]. Specifically, the competing methods include:

- Empirical Risk Minimization (**ERM**) [35] which aims to minimize the cumulative training error across all seen domains.
- Domain-Adversarial Neural Networks (**DANN**) [17] which is motivated by the theoretical results from [5]. In particular, to minimize the upper bound of the risk in the unseen domain, **DANN** adopts an adversarial network to enforce that features from different domains are indistinguishable.



- Class-conditional DANN (**C-DANN**) [26] is a variant of **DANN** that aims to match not only the feature distributions between domains but also match the conditional distributions of the label given the data across domains.
- Invariant Risk Minimization (**IRM**) [3] aims to learn features such that the optimal classifiers applied to these features are matched across domains.
- Risk Extrapolation (**VREx**) [22] is constructed on the assumption from [3] which assumes the existence of an optimal linear classifier across all domains. While **IRM** specifically seeks the invariant classifier, **VREx** aims to identify the form of the distribution shift, leading to the robustness for a wider variety of distributional shifts.
- Marginal Transfer Learning (**MTL**) [7, 6] is proposed based on an upper bound for the generalization error under the setting of an Agnostic Generative Model. Specifically, **MTL** estimates the mean embedding per domain and uses it as a second argument for optimizing the classifier.
- **CORAL** [34] is based on the idea of matching the mean and covariance of feature distributions from different domains.
- Style-Agnostic Networks (**SagNet**) [28] minimizes the style induced domain gap by randomizing the style feature for different domains and train the model mainly on the disentangled content feature.
- Adaptive Risk Minimization (**ARM**) [38] adopts meta-learning method and makes use of unlabeled data at test time for model adaptation.

We can divide the tested algorithms in [18] into two categories: (1) heuristic algorithms i.e., the algorithms that are unsupported by theoretical analysis, and (2) theory-guided algorithms. Since the proposed method in this paper belongs to the second group, we mainly compare it with the theory-guided methods. Here, **ERM** acts as the baseline theory-guided model and **DANN**, **C-DANN**, **IRM**, **VREx**, **MTL** are five state-of-the-art theory-guided algorithms. Besides these six methods, for a complete comparison, we also include three heuristic algorithms that achieve the best performances on four evaluated datasets [18]. More specific, **ARM** [38] is the best-performing algorithm for the Colored MNIST dataset, **SagNet** [28] is the best-performing algorithm for the PACS dataset, and **CORAL** [34] is the best-performing algorithm for both the VLCS and Office-Home datasets.

We use Nvidia-tesla P100 16 GB GPU for computation. The whole experiment is repeated three times with different random seeds and only the average accuracy together with its standard error are reported.

Table 1: Performance of tested methods on Colored MNIST dataset measured by accuracy (%). Here, +90%, +80%, -90% denote the degrees of correlation between colors and labels. Each degree of correlation corresponds to a domain.

Algorithm	+90%	+80%	-90%	Avg
ERM	71.7 ± 0.1	72.9 ± 0.2	10.0 ± 0.1	51.5
IRM	72.5 ± 0.1	73.3 ± 0.5	10.2 ± 0.3	52.0
DANN	71.4 ± 0.9	73.1 ± 0.1	10.0 ± 0.0	51.5
CDANN	72.0 ± 0.2	73.0 ± 0.2	10.2 ± 0.1	51.7
MTL	70.9 ± 0.2	72.8 ± 0.3	<b>10.5 ± 0.1</b>	51.4
VREx	72.4 ± 0.3	72.9 ± 0.4	10.2 ± 0.0	51.8
ARM	<b>82.0 ± 0.5</b>	<b>76.5 ± 0.3</b>	10.2 ± 0.0	<b>56.2</b>
WBAE	71.5 ± 0.3	73.4 ± 0.1	10.4 ± 0.3	51.8

Table 2: Performance of tested methods on PACS dataset measured by accuracy (%). A, C, P, S are left-out unseen domains.

Algorithm	A	C	P	S	Avg
ERM	84.7 ± 0.4	80.8 ± 0.6	97.2 ± 0.3	79.3 ± 1.0	85.5
IRM	84.8 ± 1.3	76.4 ± 1.1	96.7 ± 0.6	76.1 ± 1.0	83.5
DANN	86.4 ± 0.8	77.4 ± 0.8	<b>97.3 ± 0.4</b>	73.5 ± 2.3	83.6
CDANN	84.6 ± 1.8	75.5 ± 0.9	96.8 ± 0.3	73.5 ± 0.6	82.6
MTL	<b>87.5 ± 0.8</b>	77.1 ± 0.5	96.4 ± 0.8	77.3 ± 1.8	84.6
VREx	86.0 ± 1.6	79.1 ± 0.6	96.9 ± 0.5	77.7 ± 1.7	84.9
SagNet	87.4 ± 1.0	80.7 ± 0.6	97.1 ± 0.1	80.0 ± 0.4	86.3
WBAE	86.9 ± 0.3	<b>81.3 ± 0.4</b>	97.2 ± 0.2	<b>80.5 ± 0.4</b>	<b>86.5</b>

Table 3: Performance of tested methods on VLCS dataset measured by accuracy (%). C, L, S, V are left-out unseen domains.

Algorithm	C	L	S	V	Avg
ERM	97.7 ± 0.4	64.3 ± 0.9	73.4 ± 0.5	74.6 ± 1.3	77.5
IRM	98.6 ± 0.1	64.9 ± 0.9	73.4 ± 0.6	77.3 ± 0.9	78.5
DANN	<b>99.0 ± 0.3</b>	65.1 ± 1.4	73.1 ± 0.3	77.2 ± 0.6	78.6
CDANN	97.1 ± 0.3	65.1 ± 1.2	70.7 ± 0.8	77.1 ± 1.5	77.5
MTL	97.8 ± 0.4	64.3 ± 0.3	71.5 ± 0.7	75.3 ± 1.7	77.2
VREx	98.4 ± 0.3	64.4 ± 1.4	<b>74.1 ± 0.4</b>	76.2 ± 1.3	78.3
CORAL	98.3 ± 0.1	<b>66.1 ± 1.2</b>	73.4 ± 0.3	77.5 ± 1.2	<b>78.8</b>
WBAE	98.3 ± 0.2	65.5 ± 1.0	72.8 ± 0.3	<b>78.6 ± 0.4</b>	<b>78.8</b>

Table 4: Performance of tested methods on Office-Home dataset measured by accuracy (%). A, C, P, R are left-out unseen domains.

Algorithm	A	C	P	R	Avg
ERM	61.3 ± 0.7	52.4 ± 0.3	75.8 ± 0.1	76.6 ± 0.3	66.5
IRM	58.9 ± 2.3	52.2 ± 1.6	72.1 ± 2.9	74.0 ± 2.5	64.3
DANN	59.9 ± 1.3	53.0 ± 0.3	73.6 ± 0.7	76.9 ± 0.5	65.9
CDANN	61.5 ± 1.4	50.4 ± 2.4	74.4 ± 0.9	76.6 ± 0.8	65.8
MTL	61.5 ± 0.7	52.4 ± 0.6	74.9 ± 0.4	76.8 ± 0.4	66.4
VREx	60.7 ± 0.9	53.0 ± 0.9	75.3 ± 0.1	76.6 ± 0.5	66.4
CORAL	<b>65.3 ± 0.4</b>	54.4 ± 0.5	<b>76.5 ± 0.1</b>	78.4 ± 0.5	68.7
WBAE	63.7 ± 0.5	<b>56.4 ± 0.8</b>	76.1 ± 0.3	<b>78.8 ± 0.4</b>	<b>68.8</b>

**Results:** As shown in Table 1, 2, 3, and 4, the proposed method (WBAE) achieves comparable results with the state-of-the-art methods. In particular, WBAE obtains the highest accuracy in two out of four datasets over all methods and has a modest improvement over all theory-guided methods on PACS, VLCS, and Office-Home datasets. For the aforementioned three datasets, the proposed method also acts as good as or slightly better than the best-performing heuristic DG methods. Specifically, an improvement can be seen in Table 2 when examining the proposed method on the PACS dataset, a benchmark dataset specially designed for DG evaluation [40]. Our WBAE method outperforms the theory-guided comparison methods by 0.5% and 1.2% points in both Cartoon (C) and Sketch (S) domains and by at least 1% point on average. It also achieves a slightly better performance than the best-performing heuristic DG method by 0.2% points. A similar trend is shown in Table 3, where WBAE shows its performance gain on VLCS dataset by at least 0.2% over all theory-guided comparison methods. The effectiveness of the proposed method can be more easily observed on Office-Home, a larger and more challenging dataset, in Table 4. Particularly, compared with all theory-guided methods on Office-Home, WBAE boosts the average accuracy by at least 2.3% points on average and at least 2.2%, 3.4%, 0.3%, and 1.9% points on each task.

From the results above, we observe that the PACS and Office-Home datasets benefit more from our proposed algorithm (WBAE) than the VLCS dataset. One possible reason, as also proposed in [40], is that three out of four domains in the

VLCS dataset contain more scenery contents than the object information, which makes it hard for the feature extractor to get useful object information for domain generalization and downstream classification. In contrast, images from PACS and Office-Home datasets tend to contain objects solely, with the main differences in styles, textures, and shapes.

For the Colored MNIST dataset, WBAE does not achieve the best performance among all theory-guided methods, but is still comparable to its counterparts as shown in Table 1. The failure of our algorithm on the Colored MNIST dataset may arise from the strong spurious correlation between the colors and the image’s labels which makes the classification tasks extremely challenging. In addition, all 14 tested domain generalization algorithms in [18] also perform poorly on the Colored MNIST dataset.

#### 4.1 Ablation Study

To study the impact of different components of the loss function in Eq. (10), we conducted an ablation study for WBAE on all four datasets. In particular, we consider the following variants of our method: (1) no  $L_{bary}$ : using the WBAE loss function without the Wasserstein barycenter term  $L_{bary}$ ; (2) no  $L_r$ : using the WBAE loss function without the reconstruction term  $L_r$ . We re-ran all the experiments three times using the same model architectures, hyper-parameter tuning, and validation processes.

From Table 5, we find that removing  $L_r$  from the WBAE loss function leads to a decrease in the accuracy of around 0.3%, 0.5%, 0.4%, and 1.1% points for Colored MNIST, PACS, VLCS, and Office-Home datasets, respectively. The performance deterioration can be more clearly observed when removing  $L_{bary}$  from the WBAE loss function, leading to a drop of around 0.4%, 1.2%, 0.9%, and 3.1% points for Colored MNIST, PACS, VLCS, and Office-Home datasets, respectively. Our ablation study demonstrates the importance of the Wasserstein barycenter loss and also shows the auxiliary role of the reconstruction loss. This is reflected in the obvious performance drop when removing  $L_{bary}$  and a less significant drop when removing  $L_r$ .

Table 5: Ablation study for the proposed algorithm (WBAE) on Colored MNIST, PACS, VLCS, and Office-Home datasets.

Dataset	no $L_{bary}$	no $L_r$	WBAE
Colored MNIST	51.4 ± 0.1	51.5 ± 0.1	51.8 ± 0.2
PACS	85.3 ± 0.3	86.0 ± 0.1	86.5 ± 0.2
VLCS	77.9 ± 0.1	78.4 ± 0.2	78.8 ± 0.2
Office-Home	65.7 ± 0.2	67.7 ± 0.1	68.8 ± 0.1

## 5 CONCLUSION AND FUTURE WORK

In this paper, we revisited the theory and methods for DG and provided a new upper bound for the risk in the unseen domain. Our analysis could be potentially tightened towards understanding minimal regularity conditions on the distribution and the loss functions that can yield better bounds or a family of bounds adapted to different situations. In terms of algorithm and numerical implementation, we note that although our theory-guided method shows its effectiveness on addressing DG problem, it could be computationally expensive due to the high cost incurred in estimating the Wasserstein-2 barycenter. To alleviate this problem, our future work will focus on leveraging the recently proposed large-scale-barycenter and mapping estimators [13] to enable a larger amount of samples for barycenter calculation. Another limitation of our work lies on the backbone structure. In this paper, most of the experiments are based on ResNet-50 backbone without further exploring different model structure, like ResNet-18 or AlexNet [21]. We leave it as a feature work to explore.

#### Code Availability

The code used to generate the results and tables are available in the Github repository:

[https://github.com/boyanglyu/DG\\_via\\_WB](https://github.com/boyanglyu/DG_via_WB).

## A COMPARISON OF UPPER BOUNDS

### A.1 Shortcomings of Previously Proposed Upper Bounds

First, recall that a *domain*  $v$  is a triple  $(\mu^{(v)}, f^{(v)}, g^{(v)})$  consisting of a distribution  $\mu^{(v)}$  on the inputs  $\mathbf{x} \in \mathbb{R}^d$ , a representation function  $f^{(v)} : \mathbb{R}^d \rightarrow \mathbb{R}^{d'}$  that maps an input  $\mathbf{x}$  from input space to its representation  $\mathbf{z}$  in the representation space, and a stochastic labeling function  $g^{(v)} : \mathbb{R}^{d'} \rightarrow \mathcal{Y}$  that maps the representation space  $\mathbb{R}^{d'}$  to a label space  $\mathcal{Y}$ .

We denote the unseen domain by  $(\mu^{(u)}, f^{(u)}, g^{(u)})$  and the seen domain by  $(\mu^{(s)}, f^{(s)}, g^{(s)})$ . Let  $\mathcal{F} = \{f|f : \mathbb{R}^d \rightarrow \mathbb{R}^{d'}\}$  be a set of *representation functions*,  $\mathcal{G} = \{g|g : \mathbb{R}^{d'} \rightarrow \mathcal{Y}\}$  a set of stochastic *labeling functions*. Here, the label space  $\mathcal{Y}$  is considered as binary. A *hypothesis*  $h : \mathbb{R}^d \rightarrow \mathcal{Y}$  is obtained by composing each  $g \in \mathcal{G}$  with each  $f \in \mathcal{F}$ , *i.e.*,  $h = g \circ f$ . Next, we rewrite Theorem 1 in [5] using our notations.

**Theorem A.1.** [5] *Let  $f$  be a fixed representation function from input space to representation space and  $\mathcal{G}$  be a hypothesis space of VC-dimension  $k$ . If a random labeled sample of size  $m$  is generated by applying  $f$  to i.i.d. samples from the seen domain, then with probability at least  $1 - \delta$ , for every  $g \in \mathcal{G}$ :*

$$R^{(u)}(g) \leq R^{(s)}(g) + d_{\mathcal{H}}(f_{\#}\mu^{(u)}, f_{\#}\mu^{(s)}) + \lambda \quad (11)$$

$$\leq \hat{R}^{(s)}(g) + \sqrt{\frac{4}{m} \left( k \log \frac{2em}{k} + \log \frac{4}{\delta} \right)} + d_{\mathcal{H}}(f_{\#}\mu^{(u)}, f_{\#}\mu^{(s)}) + \lambda \quad (12)$$

where  $e$  is the base of the natural logarithm,  $d_{\mathcal{H}}$  is  $\mathcal{H}$ -divergence (please see Definition 1 in [4], Definition 2.1 in [39] or Definition 1 in [19]),  $R^{(u)}(g) = \mathbb{E}_{\mathbf{z} \sim f_{\#}\mu^{(u)}} [|g(\mathbf{z}) - g^{(u)}(\mathbf{z})|]$  denotes the risk in the unseen domain,  $R^{(s)}(g) = \mathbb{E}_{\mathbf{z} \sim f_{\#}\mu^{(s)}} [|g(\mathbf{z}) - g^{(s)}(\mathbf{z})|]$  and  $\hat{R}^{(s)}(g)$  denote the risk in the seen domain and its empirical estimation, respectively, and:

$$\lambda = \inf_{g \in \mathcal{G}} (R^{(s)}(g) + R^{(u)}(g)) \quad (13)$$

is the combined risk.

Although the bound in Theorem 1 of [5] was originally constructed for the domain adaptation problem, it has significantly influenced past and recent work in domain generalization as discussed earlier in Section 1. To highlight the differences between our work and previous theoretical bounds (the bound in Theorem 1 of [5] and Theorem 4.1 of [39]), we provide a detailed comparison below:

- First, [5] defines the risk induced by labeling function  $g$  from the representation space to the label space based on the disagreement between  $g$  and the optimal labeling function  $g^{(u)}$ :

$$R^{(u)}(g) = \mathbb{E}_{\mathbf{z} \sim f_{\#}\mu^{(u)}} [|g(\mathbf{z}) - g^{(u)}(\mathbf{z})|]. \quad (14)$$

On the other hand, we define the risk induced by using a hypothesis  $h$  from input space to label space by the disagreement between  $h$  and the optimal hypothesis  $h^{(u)}$  via a general loss function  $\ell(\cdot, \cdot)$ :

$$R^{(u)}(h) = \mathbb{E}_{\mathbf{x} \sim \mu^{(u)}} [\ell(h(\mathbf{x}), h^{(u)}(\mathbf{x}))]. \quad (15)$$

Since the empirical risk measures the probability of misclassification of a hypothesis that maps from the input space to the label space, minimizing  $R^{(u)}(g)$  does not guarantee minimizing the empirical risk. Though there are some cases for the causality to hold, for example, if the representation function  $f$  is invertible *i.e.*, there is a one-to-one mapping between  $\mathbf{x}$  and  $\mathbf{z}$ , and the loss function  $\ell(a, b) = |a - b|$ , it is possible to verify that  $R^{(u)}(g) = R^{(u)}(h)$ . In general, the representation map might not be invertible. For example, let us consider a representation function  $f$  that maps  $f(\mathbf{x}_1) = f(\mathbf{x}_2) = \mathbf{z}$ ,  $\mathbf{x}_1 \neq \mathbf{x}_2$ , with corresponding labels given by  $y_1 = 0$  and  $y_2 = 1$ . In this case, the risk defined in (14) will introduce a larger error than the risk introduced in (15) since  $g(\mathbf{z})$  cannot be mapped to both “0” and “1”. That said, the risk defined in (15) is more precise to describe the empirical risk. In addition, the risk defined in (14) is only a special case of (15) when the representation map  $f$  is invertible and the loss function satisfies  $\ell(a, b) = |a - b|$ .

- Second, using the setting in [5], for a given hypothesis space, the ideal joint hypothesis  $g^*$  is defined as the hypothesis which globally minimizes the combined error from seen and unseen domains [5, 4]:

$$g^* = \arg \min_{g \in \mathcal{G}} (R^{(s)}(g) + R^{(u)}(g)).$$

In other words, this hypothesis should work well in both domains. The error induced by using this ideal joint hypothesis is called *combined risk*:

$$\lambda = \inf_{g \in \mathcal{G}} (R^{(s)}(g) + R^{(u)}(g)) = (R^{(s)}(g^*) + R^{(u)}(g^*)).$$

Note that the labeling function  $g$  is a mapping from the representation space to the label space, therefore the ideal labeling function  $g^*$  depends implicitly on the representation function  $f$ , hence,  $\lambda$  must depend on  $f$ . Simply ignoring this fact and treating  $\lambda$  as a constant may loosen the upper bound. In contrast, our goal is to construct an upper bound with the *combined risk* term  $\sigma^{(u,s)}$  independent of both the representation function and the labeling function, which can be seen from Lemma 2.1 and Theorem 2.5.

Finally, it is worth comparing our upper bound with the bound in Theorem 4.1 of [39] which also has the *combined risk* term free of the choice of the hypothesis class. However, note that the result in Theorem 4.1 of [39] does not consider any representation function  $f$ , *i.e.*, their labeling function directly maps from the input space to the label space, while our hypothesis is composed of a representation function from input space to representation space followed by a labeling function from representation space to label space. Since it is possible to pick a representation function  $f$  that maps any input to itself, *i.e.*,  $f(\mathbf{x}) = \mathbf{x}$  which leads to  $h = g \circ f = g$ , the bound in [39] can be viewed as a special case of our proposed upper bound in Lemma 2.1.

## A.2 Comparison with Upper Bounds in [31] and [33]

The form of the upper bound derived in Theorem 2.5 shares some similarities with Lemma 1 in [31] and Theorem 1 in [33], for example, all of them introduce Wasserstein distance between domain distributions. However, they differ in the following key aspects.

1. The term containing Wasserstein distance in our upper bound is constructed in the *representation* space, not in the data (ambient) space, which provides a theoretical justification for the risk of unseen domain when decomposing the hypothesis into a representation mapping and a labeling function. This is also consistent with the algorithmic implementation in practice.
2. The bounds in Lemma 1 of [31] and Theorem 1 of [33] are controlled by the Wasserstein-1 distance while our upper bound is managed by the square-root of the Wasserstein-2 distance. There are regimes where one bound is tighter than the other. First, it is well-known that  $W_1(\mu, \nu) \leq W_2(\mu, \nu)$ , if  $W_2(\mu, \nu) \leq 1$ , then  $W_1(\mu, \nu) \leq \sqrt{W_2(\mu, \nu)}$ . However, based on Jensen's inequality, it is possible to show that  $\sqrt{W_2(\mu, \nu)} \leq [Diam(f(\mathbf{X}))W_1(\mu, \nu)]^{1/4}$  where  $Diam(f(\mathbf{X}))$  denotes the largest distance between two points in the representation space  $\mathbb{R}^{d'}$  generated by input  $\mathbf{X}$  via mapping  $f$ . To guarantee  $\sqrt{W_2(\mu, \nu)} \leq W_1(\mu, \nu)$ , a sufficient condition is  $[Diam(f(\mathbf{X}))W_1(\mu, \nu)]^{1/4} \leq W_1(\mu, \nu)$  which is equivalent to  $Diam(f(\mathbf{X})) \leq W_1(\mu, \nu)^3$ . In fact, for a given  $Diam(f(\mathbf{X}))$ , the larger the value of  $W_1(\mu, \nu)$ , the higher the chance that this sufficient condition will hold.

## B PROOFS

### B.1 Proof of Lemma 2.1

Note that in this paper, we assume that any hypothesis function  $h(\cdot)$  outputs a value in  $[0, 1]$  *i.e.*,  $h : \mathcal{R}^d \rightarrow [0, 1]$ , and  $\ell(\cdot, \cdot)$  is a bounded distance metric. In addition, we assume that  $h^{(u)}(\cdot)$  is  $K$ -Lipschitz continuous and  $\ell(\cdot)$  is  $Q$ -Lipschitz continuous. Particularly, we assume that for any  $a, b$ , and  $c$ , the following inequalities hold:

$$|h^{(u)}(a) - h^{(u)}(b)| \leq K \|a - b\|_2, \quad (16)$$

$$|\ell(a, b) - \ell(a, c)| \leq Q \|b - c\|_2, \quad (17)$$

where  $\|a - b\|_2$  and  $\|b - c\|_2$  denote the Euclidean distances between  $a$  and  $b$ , and  $b$  and  $c$ , respectively.

**Lemma 2.1.** If  $h^{(u)}(\cdot)$  is  $K$ -Lipschitz continuous and  $\ell(\cdot)$  is  $Q$ -Lipschitz continuous. Then, for any hypothesis  $h \in \mathcal{H}$  and any function (decoder)  $\psi : \mathcal{R}^{d'} \rightarrow \mathcal{R}^d$ , the following bound holds:

$$R^{(u)}(h) \leq R^{(s)}(h) + L \|f_{\#}\mu^{(u)} - f_{\#}\mu^{(s)}\|_1 + QK \left( \mathbb{E}_{\mathbf{x} \sim \mu^{(s)}} [\|\psi(f(\mathbf{x})) - \mathbf{x}\|_2] + \mathbb{E}_{\mathbf{x} \sim \mu^{(u)}} [\|\psi(f(\mathbf{x})) - \mathbf{x}\|_2] \right) + \sigma^{(u,s)}$$

where  $\|f_{\#}\mu^{(u)} - f_{\#}\mu^{(s)}\|_1 = \int_{\mathbf{z}} |f_{\#}\mu^{(u)} - f_{\#}\mu^{(s)}| d\mathbf{z}$  denotes the  $L^1$  distance between  $(f_{\#}\mu^{(u)}, f_{\#}\mu^{(s)})$  and:

$$\sigma^{(u,s)} := \min \{ \mathbb{E}_{\mathbf{x} \sim \mu^{(u)}} [\ell(h^{(u)}(\mathbf{x}), h^{(s)}(\mathbf{x}))], \mathbb{E}_{\mathbf{x} \sim \mu^{(s)}} [\ell(h^{(u)}(\mathbf{x}), h^{(s)}(\mathbf{x}))] \}.$$

*Proof.* First, we want to note that our approach is motivated by the proof of Theorem 1 in [4]. Next, to better demonstrate the relationship between the hypothesis, input distribution, true representation and labeling functions, we use inner product notation  $\langle \cdot, \cdot \rangle$  to denote expectations. Specifically,

$$R^{(v)}(h) := \mathbb{E}_{\mathbf{x} \sim \mu^{(v)}} [\ell(h(\mathbf{x}), h^{(v)}(\mathbf{x}))] = \langle \ell(h, h^{(v)}), \mu^{(v)} \rangle. \quad (18)$$

From the definition of risk,

$$\begin{aligned} R^{(u)}(h) &= \langle \ell(h, h^{(u)}), \mu^{(u)} \rangle = \langle \ell(h, h^{(s)}), \mu^{(s)} \rangle - \langle \ell(h, h^{(s)}), \mu^{(s)} \rangle + \langle \ell(h, h^{(u)}), \mu^{(u)} \rangle \\ &= R^{(s)}(h) + (\langle \ell(h, h^{(u)}), \mu^{(u)} \rangle - \langle \ell(h, h^{(s)}), \mu^{(u)} \rangle) + (\langle \ell(h, h^{(s)}), \mu^{(u)} \rangle - \langle \ell(h, h^{(s)}), \mu^{(s)} \rangle) \\ &\leq R^{(s)}(h) + \langle \ell(h^{(u)}, h^{(s)}), \mu^{(u)} \rangle + \langle \ell(h, h^{(s)}), \mu^{(u)} - \mu^{(s)} \rangle \end{aligned} \quad (19)$$

where (19) follows from the triangle inequality  $\ell(h, h^{(u)}) \leq \ell(h, h^{(s)}) + \ell(h^{(s)}, h^{(u)})$  and because  $\ell(h^{(s)}, h^{(u)}) = \ell(h^{(u)}, h^{(s)})$ .

In an analogous fashion, it is possible to show that:

$$R^{(u)}(h) \leq R^{(s)}(h) + \langle \ell(h^{(u)}, h^{(s)}), \mu^{(s)} \rangle + \langle \ell(h, h^{(u)}), \mu^{(u)} - \mu^{(s)} \rangle. \quad (20)$$

Next, we will bound the third term in the right-hand-side of (20). Specifically,

$$\begin{aligned} &\langle \ell(h, h^{(u)}), \mu^{(u)} - \mu^{(s)} \rangle \\ &= \mathbb{E}_{\mathbf{x} \sim \mu^{(u)}} [\ell(h(\mathbf{x}), h^{(u)}(\mathbf{x}))] - \mathbb{E}_{\mathbf{x} \sim \mu^{(s)}} [\ell(h(\mathbf{x}), h^{(u)}(\mathbf{x}))] \\ &\leq \max \left\{ \mathbb{E}_{\mathbf{x} \sim \mu^{(u)}} [\ell(h(\mathbf{x}), h^{(u)}(\psi(f(\mathbf{x}))) + K\|\psi(f(\mathbf{x})) - \mathbf{x}\|_2)], \mathbb{E}_{\mathbf{x} \sim \mu^{(u)}} [\ell(h(\mathbf{x}), h^{(u)}(\psi(f(\mathbf{x}))) - K\|\psi(f(\mathbf{x})) - \mathbf{x}\|_2)] \right\} \\ &\quad - \min \left\{ \mathbb{E}_{\mathbf{x} \sim \mu^{(s)}} [\ell(h(\mathbf{x}), h^{(u)}(\psi(f(\mathbf{x}))) + K\|\psi(f(\mathbf{x})) - \mathbf{x}\|_2)], \mathbb{E}_{\mathbf{x} \sim \mu^{(s)}} [\ell(h(\mathbf{x}), h^{(u)}(\psi(f(\mathbf{x}))) - K\|\psi(f(\mathbf{x})) - \mathbf{x}\|_2)] \right\} \end{aligned} \quad (21)$$

$$\begin{aligned} &\leq \left( \mathbb{E}_{\mathbf{x} \sim \mu^{(u)}} [\ell(h(\mathbf{x}), h^{(u)}(\psi(f(\mathbf{x}))))] + \mathbb{E}_{\mathbf{x} \sim \mu^{(u)}} [QK\|\psi(f(\mathbf{x})) - \mathbf{x}\|_2] \right) \\ &\quad - \left( \mathbb{E}_{\mathbf{x} \sim \mu^{(s)}} [\ell(h(\mathbf{x}), h^{(u)}(\psi(f(\mathbf{x}))))] - \mathbb{E}_{\mathbf{x} \sim \mu^{(s)}} [QK\|\psi(f(\mathbf{x})) - \mathbf{x}\|_2] \right) \end{aligned} \quad (22)$$

$$\begin{aligned} &= \mathbb{E}_{\mathbf{z} \sim f_{\#} \mu^{(u)}} [\ell(g(\mathbf{z}), h^{(u)}(\psi(\mathbf{z})))] - \mathbb{E}_{\mathbf{z} \sim f_{\#} \mu^{(s)}} [\ell(g(\mathbf{z}), h^{(u)}(\psi(\mathbf{z})))] \\ &\quad + \mathbb{E}_{\mathbf{x} \sim \mu^{(u)}} [QK\|\psi(f(\mathbf{x})) - \mathbf{x}\|_2] + \mathbb{E}_{\mathbf{x} \sim \mu^{(s)}} [QK\|\psi(f(\mathbf{x})) - \mathbf{x}\|_2] \end{aligned} \quad (23)$$

$$\begin{aligned} &= \langle \ell(g(\mathbf{z}), h^{(u)}(\psi(\mathbf{z}))), f_{\#} \mu^{(u)} - f_{\#} \mu^{(s)} \rangle + QK \left( \mathbb{E}_{\mathbf{x} \sim \mu^{(s)}} [\|\psi(f(\mathbf{x})) - \mathbf{x}\|_2] + \mathbb{E}_{\mathbf{x} \sim \mu^{(u)}} [\|\psi(f(\mathbf{x})) - \mathbf{x}\|_2] \right) \\ &\leq L \langle 1, |f_{\#} \mu^{(u)} - f_{\#} \mu^{(s)}| \rangle + QK \left( \mathbb{E}_{\mathbf{x} \sim \mu^{(s)}} [\|\psi(f(\mathbf{x})) - \mathbf{x}\|_2] + \mathbb{E}_{\mathbf{x} \sim \mu^{(u)}} [\|\psi(f(\mathbf{x})) - \mathbf{x}\|_2] \right). \end{aligned} \quad (24)$$

Note that in this paper, any hypothesis function  $h(\cdot)$  is assumed to output a scalar value in  $[0, 1]$ , i.e.,  $h : \mathcal{R}^d \rightarrow [0, 1]$ , and  $\ell(\cdot, \cdot)$  is a distance metric. With all these assumptions, we get (21) due to  $\min\{\ell(a, c), \ell(a, d)\} \leq \ell(a, b) \leq \max\{\ell(a, c), \ell(a, d)\}$ ,  $\forall b \in [c, d]$ ,  $a, b, c, d \in \mathcal{R}$  and the fact for Lipschitz function  $h^{(u)}(\cdot)$  that:

$$h^{(u)}(\psi(f(\mathbf{x}))) - K\|\psi(f(\mathbf{x})) - \mathbf{x}\|_2 \leq h^{(u)}(\mathbf{x}) \leq h^{(u)}(\psi(f(\mathbf{x}))) + K\|\psi(f(\mathbf{x})) - \mathbf{x}\|_2. \quad (25)$$

Next, (22) is due to the Lipschitzness of  $\ell(\cdot)$ :

$$\begin{aligned} &\max \left\{ \ell(h(\mathbf{x}), h^{(u)}(\psi(f(\mathbf{x}))) + K\|\psi(f(\mathbf{x})) - \mathbf{x}\|_2), \ell(h(\mathbf{x}), h^{(u)}(\psi(f(\mathbf{x}))) - K\|\psi(f(\mathbf{x})) - \mathbf{x}\|_2) \right\} \\ &\leq \ell(h(\mathbf{x}), h^{(u)}(\psi(f(\mathbf{x})))) + QK\|\psi(f(\mathbf{x})) - \mathbf{x}\|_2, \end{aligned} \quad (26)$$

$$\begin{aligned} &\min \left\{ \ell(h(\mathbf{x}), h^{(u)}(\psi(f(\mathbf{x}))) + K\|\psi(f(\mathbf{x})) - \mathbf{x}\|_2), \ell(h(\mathbf{x}), h^{(u)}(\psi(f(\mathbf{x}))) - K\|\psi(f(\mathbf{x})) - \mathbf{x}\|_2) \right\} \\ &\geq \ell(h(\mathbf{x}), h^{(u)}(\psi(f(\mathbf{x})))) - QK\|\psi(f(\mathbf{x})) - \mathbf{x}\|_2. \end{aligned} \quad (27)$$

Finally, we get (23) due to  $h = g \circ f$ ,  $f(\mathbf{x}) = \mathbf{z}$ , and (24) due to  $\ell(\cdot, \cdot)$  is bounded by  $L$ .

The proof of Lemma follows by combining (19), (20), (24), and note that:

$$\sigma^{(u,s)} = \min \left\{ \langle \ell(h^{(u)}, h^{(s)}), \mu^{(u)} \rangle, \langle \ell(h^{(u)}, h^{(s)}), \mu^{(s)} \rangle \right\},$$

and

$$\langle 1, |f_{\#} \mu^{(u)} - f_{\#} \mu^{(s)}| \rangle = \|f_{\#} \mu^{(u)} - f_{\#} \mu^{(s)}\|_1.$$

□

## B.2 Proof of Lemma 2.4

From Pinsker's inequality [8], the  $L^1$  distance can be bounded by Kullback–Leibler (KL) divergence as follows:

$$\|\mu - \nu\|_1^2 \leq 2d_{KL}(\mu, \nu) \quad (28)$$

where  $\|\mu - \nu\|_1$  and  $d_{KL}(\mu, \nu)$  denote  $L^1$  distance and Kullback–Leibler divergence between two distributions  $\mu$  and  $\nu$ , respectively. Since  $\|\mu - \nu\|_1 = \|\nu - \mu\|_1$ , using Pinsker's inequality for  $(\mu, \nu)$  and  $(\nu, \mu)$ ,

$$2\|\mu - \nu\|_1^2 = \|\mu - \nu\|_1^2 + \|\nu - \mu\|_1^2 \leq 2d_{KL}(\mu, \nu) + 2d_{KL}(\nu, \mu) \quad (29)$$

which is equivalent to,

$$\|\mu - \nu\|_1 \leq \sqrt{d_{KL}(\mu, \nu) + d_{KL}(\nu, \mu)}. \quad (30)$$

Next, if  $\mu$  and  $\nu$  are  $(c_1, c_2)$ -regular distributions, their Kullback–Leibler divergences can be bounded by their Wasserstein-2 distance as follows (please see equation (10), Proposition 1 in [30]),

$$d_{KL}(\mu, \nu) + d_{KL}(\nu, \mu) \leq 2\left(\frac{c_1}{2}\sqrt{\mathbb{E}_{\mathbf{u} \sim \mu}[\|\mathbf{u}\|_2^2]} + \frac{c_1}{2}\sqrt{\mathbb{E}_{\mathbf{v} \sim \nu}[\|\mathbf{v}\|_2^2]} + c_2\right) [\mathbf{W}_2(\mu, \nu)]. \quad (31)$$

Combining (30) and (31),

$$\|\mu - \nu\|_1 \leq \sqrt{c_1\left(\sqrt{\mathbb{E}_{\mathbf{u} \sim \mu}[\|\mathbf{u}\|_2^2]} + \sqrt{\mathbb{E}_{\mathbf{v} \sim \nu}[\|\mathbf{v}\|_2^2]}\right) + 2c_2} [\mathbf{W}_2(\mu, \nu)]^{1/2}. \quad (32)$$

## B.3 Proof of Theorem 2.5

Under the assumption that  $f_{\#}\mu^{(s)}$  and  $f_{\#}\mu^{(u)}$  are  $(c_1, c_2)$ -regular  $\forall s = 1, 2, \dots, S$ , from Lemma 2.4,

$$\begin{aligned} \|f_{\#}\mu^{(u)} - f_{\#}\mu^{(s)}\|_1 &\leq \sqrt{c_1\left(\sqrt{\mathbb{E}_{\mathbf{x} \sim \mu^{(s)}}[\|f(\mathbf{x})\|_2^2]} + \sqrt{\mathbb{E}_{\mathbf{x} \sim \mu^{(u)}}[\|f(\mathbf{x})\|_2^2]}\right) + 2c_2} \\ &\quad \times [\mathbf{W}_2(f_{\#}\mu^{(u)}, f_{\#}\mu^{(s)})]^{1/2}. \end{aligned} \quad (33)$$

Let:

$$C := \max_{s \in \{1, \dots, S\}} \sqrt{c_1\left(\sqrt{\mathbb{E}_{\mathbf{x} \sim \mu^{(s)}}[\|f(\mathbf{x})\|_2^2]} + \sqrt{\mathbb{E}_{\mathbf{x} \sim \mu^{(u)}}[\|f(\mathbf{x})\|_2^2]}\right) + 2c_2}. \quad (34)$$

Multiplying (33) by  $\lambda^{(s)}$  and summing over all  $s$  we get:

$$\sum_{s=1}^S \lambda^{(s)} \|f_{\#}\mu^{(u)} - f_{\#}\mu^{(s)}\|_1 \leq C \sum_{s=1}^S \lambda^{(s)} [\mathbf{W}_2(f_{\#}\mu^{(u)}, f_{\#}\mu^{(s)})]^{1/2}. \quad (35)$$

By Jensen's inequality,

$$\sum_{s=1}^S \lambda^{(s)} [\mathbf{W}_2(f_{\#}\mu^{(u)}, f_{\#}\mu^{(s)})]^{1/2} \leq \left[\sum_{s=1}^S \lambda^{(s)} \mathbf{W}_2^2(f_{\#}\mu^{(u)}, f_{\#}\mu^{(s)})\right]^{1/4}. \quad (36)$$

From (35) and (36),

$$\sum_{s=1}^S \lambda^{(s)} \|f_{\#}\mu^{(u)} - f_{\#}\mu^{(s)}\|_1 \leq C \left[\sum_{s=1}^S \lambda^{(s)} \mathbf{W}_2^2(f_{\#}\mu^{(u)}, f_{\#}\mu^{(s)})\right]^{1/4}. \quad (37)$$

Finally, combining the upper bound in Lemma 2.2 and (37), the proof follows.

## B.4 Proof of Corollary 2.6

We begin with the second term in the upper bound of Theorem 2.5. Indeed, for any arbitrary pushforward distribution  $f_{\#}\mu$ , we have:

$$\left[ \sum_{s=1}^S \lambda^{(s)} W_2^2(f_{\#}\mu^{(u)}, f_{\#}\mu^{(s)}) \right]^{1/4} \quad (38)$$

$$\leq \left[ \sum_{s=1}^S \lambda^{(s)} \left( W_2^2(f_{\#}\mu^{(u)}, f_{\#}\mu) + W_2^2(f_{\#}\mu, f_{\#}\mu^{(s)}) \right) \right]^{1/4} \quad (39)$$

$$= \left[ \sum_{s=1}^S \lambda^{(s)} W_2^2(f_{\#}\mu^{(u)}, f_{\#}\mu) + \sum_{s=1}^S \lambda^{(s)} W_2^2(f_{\#}\mu, f_{\#}\mu^{(s)}) \right]^{1/4} \quad (40)$$

$$= \left[ W_2^2(f_{\#}\mu^{(u)}, f_{\#}\mu) + \sum_{s=1}^S \lambda^{(s)} W_2^2(f_{\#}\mu, f_{\#}\mu^{(s)}) \right]^{1/4} \quad (41)$$

$$\leq \left[ \sum_{s=1}^S \lambda^{(s)} W_2^2(f_{\#}\mu, f_{\#}\mu^{(s)}) \right]^{1/4} + \left[ W_2^2(f_{\#}\mu^{(u)}, f_{\#}\mu) \right]^{1/4} \quad (42)$$

with (39) due to the triangle inequality, (41) due to  $\sum_{s=1}^S \lambda^{(s)} = 1$ , (42) due to the fact that for any  $a, b \geq 0$  and  $0 < p \leq 1$ ,  $(a + b)^p \leq a^p + b^p$ .

Combining Theorem 2.5 and Eq. (42), the proof of Corollary 2.6 follows.

## C ARCHITECTURE AND HYPE-PARAMETERS

- The model structure of the decoder used in the Colored MNIST dataset can be found in Table 6.
- The model structure of the decoder used in the PACS, VLCS, and Office-Home datasets can be found in Table 7.
- A list of hyper-parameters used in our proposed method is shown in Table 8.

Table 6: Model structure of the decoder used for Colored MNIST dataset.

Layer
ConvTranspose2d (in=128, out=128, kernel_size=14, stride=1, padding=0)
ConvTranspose2d (in=128, out=128, kernel_size=3, stride=1, padding=1)
ReLU
ConvTranspose2d (in=128, out=128, kernel_size=3, stride=1, padding=1)
ReLU
ConvTranspose2d (in=128, out=64, kernel_size=3, stride=2, padding=1)
ReLU
ConvTranspose2d (in=64, out=2, kernel_size=3, stride=1, padding=1)
Interpolate (size=(28, 28))



Table 7: Model structure of the decoder used for PACS, VLCS, and Office-Home datasets.

Layer
ConvTranspose2d (in=2048, out=512, kernel_size=4, stride= 1, padding=0)
BatchNorm2d + ReLU
ConvTranspose2d (in=512, out=256, kernel_size=4, stride=2, padding=1)
BatchNorm2d + ReLU
ConvTranspose2d (in=256, out=128, kernel_size=4, stride=2, padding=1)
BatchNorm2d + ReLU
ConvTranspose2d (in=128, out=64, kernel_size=4, stride=2, padding=1)
BatchNorm2d + ReLU
ConvTranspose2d (in=64, out=32, kernel_size=4, stride=2, padding=1)
BatchNorm2d + ReLU
ConvTranspose2d (in=32, out=3, kernel_size=4, stride=2, padding=1)
Tanh + Interpolate (size=(224, 224))

Table 8: Hyper-parameters of the proposed method.

Parameters	Colored MNIST	PACS, VLCS and Office-Home
learning rate	0.001	0.00005
batch size	64	32
ResNet dropout	-	0
weight decay	0	0
training steps	5000	2000
$\epsilon$	20	20
$\alpha$	$10^{\text{Uniform}(-3.5, -2)}$	$10^{\text{Uniform}(-3.5, -2)}$
$\beta$	$10^{\text{Uniform}(-3.5, -1.5)}$	$10^{\text{Uniform}(-3.5, -1.5)}$

## References

- [1] Martial Agueh and Guillaume Carlier. Barycenters in the Wasserstein space. *SIAM Journal on Mathematical Analysis*, 43(2):904–924, 2011.
- [2] Isabela Albuquerque, João Monteiro, Mohammad Darvishi, Tiago H Falk, and Ioannis Mitliagkas. Generalizing to unseen domains via distribution matching. *arXiv preprint arXiv:1911.00804*, 2019.
- [3] Martin Arjovsky, Léon Bottou, Ishaan Gulrajani, and David Lopez-Paz. Invariant risk minimization. *arXiv preprint arXiv:1907.02893*, 2019.
- [4] Shai Ben-David, John Blitzer, Koby Crammer, Alex Kulesza, Fernando Pereira, and Jennifer Wortman Vaughan. A theory of learning from different domains. *Machine learning*, 79(1):151–175, 2010.
- [5] Shai Ben-David, John Blitzer, Koby Crammer, Fernando Pereira, et al. Analysis of representations for domain adaptation. *Advances in neural information processing systems*, 19:137, 2007.
- [6] Gilles Blanchard, Aniket Anand Deshmukh, Urun Dogan, Gyemin Lee, and Clayton Scott. Domain generalization by marginal transfer learning. *Journal of machine learning research*, 2021.
- [7] Gilles Blanchard, Gyemin Lee, and Clayton Scott. Generalizing from several related classification tasks to a new unlabeled sample. *Advances in neural information processing systems*, 24:2178–2186, 2011.
- [8] Imre Csiszár and János Körner. *Information theory: coding theorems for discrete memoryless systems*. Cambridge University Press, 2011.
- [9] Yuqi Cui, Yifan Xu, and Dongrui Wu. EEG-based driver drowsiness estimation using feature weighted episodic training. *IEEE transactions on neural systems and rehabilitation engineering*, 27(11):2263–2273, 2019.
- [10] Marco Cuturi. Sinkhorn distances: Lightspeed computation of optimal transport. *Advances in neural information processing systems*, 26:2292–2300, 2013.
- [11] Marco Cuturi and Arnaud Doucet. Fast computation of wasserstein barycenters. In *International conference on machine learning*, pages 685–693. PMLR, 2014.
- [12] Qi Dou, Daniel Coelho de Castro, Konstantinos Kamnitsas, and Ben Glocker. Domain generalization via model-agnostic learning of semantic features. *Advances in Neural Information Processing Systems*, 32, 2019.

- [13] Jiaojiao Fan, Amirhossein Taghvaei, and Yongxin Chen. Scalable computations of wasserstein barycenter via input convex neural networks. In *International Conference on Machine Learning*, pages 1571–1581. PMLR, 2021.
- [14] Chen Fang, Ye Xu, and Daniel N Rockmore. Unbiased metric learning: On the utilization of multiple datasets and web images for softening bias. In *Proceedings of the IEEE International Conference on Computer Vision*, pages 1657–1664, 2013.
- [15] Jean Feydy, Thibault Séjourné, François-Xavier Vialard, Shun-ichi Amari, Alain Trounev, and Gabriel Peyré. Interpolating between optimal transport and MMD using sinkhorn divergences. In *The 22nd International Conference on Artificial Intelligence and Statistics*, pages 2681–2690, 2019.
- [16] Rémi Flamary, Nicolas Courty, Alexandre Gramfort, Mokhtar Z. Alaya, Aurélie Boisbunon, Stanislas Chambon, Laetitia Chapel, Adrien Corenflos, Kilian Fatras, Nemo Fournier, Léo Gautheron, Nathalie T.H. Gayraud, Hicham Janati, Alain Rakotomamonjy, Ievgen Redko, Antoine Rolet, Antony Schutz, Vivien Seguy, Danica J. Sutherland, Romain Tavenard, Alexander Tong, and Titouan Vayer. Pot: Python optimal transport. *Journal of Machine Learning Research*, 22(78):1–8, 2021.
- [17] Yaroslav Ganin, Evgeniya Ustinova, Hana Ajakan, Pascal Germain, Hugo Larochelle, François Laviolette, Mario Marchand, and Victor Lempitsky. Domain-adversarial training of neural networks. *The journal of machine learning research*, 17(1):2096–2030, 2016.
- [18] Ishaan Gulrajani and David Lopez-Paz. In search of lost domain generalization. In *International Conference on Learning Representations*, 2021.
- [19] Daniel Kifer, Shai Ben-David, and Johannes Gehrke. Detecting change in data streams. In *VLDB*, volume 4, pages 180–191. Toronto, Canada, 2004.
- [20] Diederik P. Kingma and Jimmy Ba. Adam: A method for stochastic optimization. In Yoshua Bengio and Yann LeCun, editors, *3rd International Conference on Learning Representations, ICLR 2015, San Diego, CA, USA, May 7-9, 2015, Conference Track Proceedings*, 2015.
- [21] Alex Krizhevsky, Ilya Sutskever, and Geoffrey E Hinton. Imagenet classification with deep convolutional neural networks. *Communications of the ACM*, 60(6):84–90, 2017.
- [22] David Krueger, Ethan Caballero, Joern-Henrik Jacobsen, Amy Zhang, Jonathan Binas, Dinghuai Zhang, Remi Le Priol, and Aaron Courville. Out-of-distribution generalization via risk extrapolation (rex). In *International Conference on Machine Learning*, pages 5815–5826. PMLR, 2021.
- [23] Yann LeCun. The mnist database of handwritten digits. <http://yann.lecun.com/exdb/mnist/>, 1998.
- [24] Da Li, Yongxin Yang, Yi-Zhe Song, and Timothy M Hospedales. Deeper, broader and artier domain generalization. In *Proceedings of the IEEE international conference on computer vision*, pages 5542–5550, 2017.
- [25] Haoliang Li, Sinno Jialin Pan, Shiqi Wang, and Alex C Kot. Domain generalization with adversarial feature learning. In *Proceedings of the IEEE Conference on Computer Vision and Pattern Recognition*, pages 5400–5409, 2018.
- [26] Ya Li, Xinmei Tian, Mingming Gong, Yajing Liu, Tongliang Liu, Kun Zhang, and Dacheng Tao. Deep domain generalization via conditional invariant adversarial networks. In *Proceedings of the European Conference on Computer Vision (ECCV)*, pages 624–639, 2018.
- [27] Boyang Lyu, Thao Pham, Giles Blaney, Zachary Haga, Angelo Sassaroli, Sergio Fantini, and Shuchin Aeron. Domain adaptation for robust workload level alignment between sessions and subjects using fNIRS. *Journal of Biomedical Optics*, 26(2):1 – 21, 2021.
- [28] Hyeonseob Nam, HyunJae Lee, Jongchan Park, Wonjun Yoon, and Donggeun Yoo. Reducing domain gap by reducing style bias. In *Proceedings of the IEEE/CVF Conference on Computer Vision and Pattern Recognition*, pages 8690–8699, 2021.
- [29] Gabriel Peyré, Marco Cuturi, et al. Computational optimal transport: With applications to data science. *Foundations and Trends® in Machine Learning*, 11(5-6):355–607, 2019.
- [30] Yury Polyanskiy and Yihong Wu. Wasserstein continuity of entropy and outer bounds for interference channels. *IEEE Transactions on Information Theory*, 62(7):3992–4002, 2016.
- [31] Ievgen Redko, Amaury Habrard, and Marc Sebban. Theoretical analysis of domain adaptation with optimal transport. In *Joint European Conference on Machine Learning and Knowledge Discovery in Databases*, pages 737–753. Springer, 2017.
- [32] Filippo Santambrogio. *Optimal Transport for Applied Mathematicians: Calculus of Variations, PDEs and Modeling*. Springer, 2015.

- [33] Jian Shen, Yanru Qu, Weinan Zhang, and Yong Yu. Wasserstein distance guided representation learning for domain adaptation. In *Thirty-Second AAAI Conference on Artificial Intelligence*, 2018.
- [34] Baochen Sun and Kate Saenko. Deep coral: Correlation alignment for deep domain adaptation. In *European conference on computer vision*, pages 443–450. Springer, 2016.
- [35] Vladimir N Vapnik. An overview of statistical learning theory. *IEEE transactions on neural networks*, 10(5):988–999, 1999.
- [36] Hemanth Venkateswara, Jose Eusebio, Shayok Chakraborty, and Sethuraman Panchanathan. Deep hashing network for unsupervised domain adaptation. In *Proceedings of the IEEE conference on computer vision and pattern recognition*, pages 5018–5027, 2017.
- [37] Yifan Wu, Ezra Winston, Divyansh Kaushik, and Zachary Lipton. Domain adaptation with asymmetrically-relaxed distribution alignment. In *International conference on machine learning*, pages 6872–6881. PMLR, 2019.
- [38] Marvin Zhang, Henrik Marklund, Nikita Dhawan, Abhishek Gupta, Sergey Levine, and Chelsea Finn. Adaptive risk minimization: Learning to adapt to domain shift. *Advances in Neural Information Processing Systems*, 34:23664–23678, 2021.
- [39] Han Zhao, Remi Tachet Des Combes, Kun Zhang, and Geoffrey Gordon. On learning invariant representations for domain adaptation. In *International Conference on Machine Learning*, pages 7523–7532. PMLR, 2019.
- [40] Shanshan Zhao, Mingming Gong, Tongliang Liu, Huan Fu, and Dacheng Tao. Domain generalization via entropy regularization. *Advances in Neural Information Processing Systems*, 33, 2020.
- [41] Fan Zhou, Zhuqing Jiang, Changjian Shui, Boyu Wang, and Brahim Chaib-draa. Domain generalization via optimal transport with metric similarity learning. *Neurocomputing*, 456:469–480, 2021.
- [42] Kaiyang Zhou, Ziwei Liu, Yu Qiao, Tao Xiang, and Chen Change Loy. Domain generalization: A survey. *IEEE Transactions on Pattern Analysis and Machine Intelligence*, 2022.